Available online at www.sciencedirect.com
SCIENCE DIRECT®
Journal of Catalysis 213 (2003) 135–150
JOURNAL OF CATALYSIS
www.elsevier.com/locate/jcat

Kinetics of selective CO oxidation in excess of H_2 over the nanostructured $Cu_{0.1}Ce_{0.9}O_{2-y}$ catalyst

Gregor Sedmak,[a] Stanko Hočevar,[a,*] and Janez Levec [a,b]

[a] *Laboratory of Catalysis and Reaction Engineering, National Institute of Chemistry, Hajdrihova 19, SI-1000 Ljubljana, Slovenia*
[b] *Department of Chemistry and Chemical Technology, University of Ljubljana, Hajdrihova 19, SI-1000 Ljubljana, Slovenia*

Received 21 March 2002; revised 17 June 2002; accepted 16 September 2002

Abstract

The kinetics of CO oxidation in excess hydrogen over a nanostructured $Cu_{0.1}Ce_{0.9}O_{2-y}$ catalyst prepared by a sol–gel method was studied under simulated preferential oxidation (PROX) reactor conditions. Reaction temperature was varied between 45 and 155 °C. The partial pressures of CO and O_2 in 0.5 bar excess of H_2 and He as a balance gas were varied between 0.001 and 0.025 and between 0.001 and 0.05 bar, respectively. The catalyst was found to be 100% selective in the temperature range from 45 to 90 °C. In this temperature range, the kinetics of the reaction was found to follow the redox mechanism represented by the Mars and van Krevelen type of rate equation. Kinetic parameters of the reaction calculated on the basis of this rate equation were found to be as follows: apparent activation energy for CO oxidation step, 57.2 kJ/mol, and for the catalyst reoxidation step, 60.2 kJ/mol. The observed reaction rate at the 0.01-bar CO partial pressure and stoichiometric O_2 partial pressure at 90 °C was 2.7×10^{-6} mol/g_{cat} s. The steady-state experimental data could be regressed almost equally well with the modified Langmuir–Hinshelwood model introduced by Liu et al. However, the transient experiments performed in our study reveal that lattice oxygen could be involved even at low reaction temperatures, thus favoring the use of a steady state Mars and van Krevelen kinetic model.

Keywords: Kinetics; Catalysis; Heterogeneous; Oxidation; Selective; CO; H_2; Fuel cell; Nanostructured; CuO/CeO_2

1. Introduction

Selective oxidation of CO in excess hydrogen (also preferential oxidation, PROX) has attracted renewed interest over the last years due to its use in low-temperature proton exchange membrane fuel cell (PEMFC) technology. In order to avoid problems associated with hydrogen distribution and storage, particularly in vehicle applications, H_2 can be produced on-board by autothermal reforming of hydrocarbon fuels, preferably renewable ones, such as methanol. The gas at the outlet of a reformer and two-stage water gas-shift (WGS) reactor typically contains 45–75 vol.% H_2, 15–25 vol.% CO_2, a few vol.% H_2O, traces of unconverted fuel and, unfortunately, 0.5–2 vol.% CO, which is a catalyst poison for the fuel cell Pt gas diffusion anode. It is imperative to lower the concentration of CO in the reformer gas below 100 ppm, a concentration tolerable by modern Pt alloy electrocatalysts.

Nowadays operating PROX reactor catalysts are prepared from costly alumina-supported Pt, Pd, Ru, and Rh, which operate at temperatures of 150–200 °C and significantly lose selectivity at those temperatures. In order to keep the overall energy conversion process as efficient as possible, the CO oxidation must be highly selective. Namely, the formation of water reduces the amount of hydrogen needed to operate the fuel cell and reduces its energy conversion efficiency [1].

From a process point of view (reformer → two-stage WGS reactor → PROX → fuel cell) there are two temperature levels which are particularly convenient for a PROX reactor: either the PEMFC operating temperature (80–100 °C) or the temperature of the methanol reformer unit (250–300 °C) [2,3]. The other crucial requirement for the PROX reactor is a high oxidation rate of CO. The reaction rate over 3 wt.% Au finely dispersed on α-Fe_2O_3 at 30 °C and $P_{CO} = P_{O_2} = 1$ kPa, where the selectivity is 100% and CO conver-

* Corresponding author.
E-mail address: stanko.hocevar@ki.si (S. Hočevar).

0021-9517/02/$ – see front matter
PII: S0021-9517(02)00019-2

sion is over 90%, is reported to be 5.1×10^{-6} mol/g_{cat} s. It must be noted, however, that when the temperature is raised to the PEMFC working temperature, the selectivity drops to only 40%. The reaction rate over 0.5 wt.% Pt finely dispersed on γ-Al_2O_3 at 200 °C and at the same partial pressures of CO and O_2, where the maximum selectivity is around 40% and CO conversion 100%, is reported to be 5.2×10^{-6} mol/g_{cat} s [2,3]. A two-stage CO selective oxidation reactor for PEMFC automotive applications based on a wash-coat Pt and Ru/Al_2O_3 catalyst and on a compact fin heat exchanger design has a volume of 1 L in order to lower the initial CO concentration in the reformer fuel of 0.5% down to less than 20 ppm at 160 °C and a gas hourly space velocity (GHSV) of 19,000 h^{-1}, i.e., at fuel flow rate equivalent to a PEMFC electrical power output of 5 kW_{el} [4].

In order to lower the cost and improve the selectivity of the catalyst, a novel nonstoichiometric nanostructured $Cu_{0.1}Ce_{0.9}O_{2-y}$ catalyst for the selective low-temperature oxidation of CO in excess H_2 was synthesized by coprecipitation and by sol–gel methods and patented [5,6]. The sol–gel method of catalyst preparation is particularly convenient for deposition on diverse geometries of support (i.e., honeycomb supports) and/or reactors, which can be used in PROX processes. The activity and selectivity of the $Cu_{0.05}Ce_{0.95}O_{2-y}$ catalyst prepared by coprecipitation methods was compared to the Pt/γ-Al_2O_3 and Au/α-Fe_2O_3 catalysts [3]. It was found that nanostructured $Cu_{0.05}Ce_{0.95}O_{2-y}$ catalyst is superior to the other two catalysts in the low-temperature range, because it has the best compromise between activity, selectivity, and price of the catalyst. This type of catalyst is also able to convert methanol directly into hydrogen and CO_2 by steam reforming through a water-gas shift reaction [7,8]. By the use of this catalyst, the four previously mentioned reactors (reformer, two-stage WGS reactor, and PROX reactor) could be incorporated into a single unit. Besides, it was shown that this type of catalyst could also be used in other environmental applications, for instance in wet oxidation of phenol [9,10], methane oxidation, and sulfur dioxide reduction [11].

In this paper we report on the kinetics of selective CO oxidation in excess hydrogen over the nanostructured $Cu_{0.1}Ce_{0.9}O_{2-y}$ catalyst as obtained in the fixed bed reactor operating in a differential mode. The reported values of rate constants and of the apparent activation energies determined in the intrinsic rate equation based on the Mars and van Krevelen mechanism reflect the inlet gaseous mixture composition. The latter simulates the real composition at the outlet of the low-temperature water gas shift reactor concerning the concentrations of CO, H_2, and O_2, but no CO_2, H_2O, or unconverted CH_3OH was present. The influence of the presence of 15% CO_2 and 10% H_2O in the reactor inlet composition on the selective CO oxidation in the excess of hydrogen was qualitatively evaluated in our previous studies [3,6]. A detailed kinetic study of the influence of those two components present in the reactor feed is left to future work.

Besides the kinetics of the selective CO oxidation we report also on the total reducibility of the $Cu_{0.1}Ce_{0.9}O_{2-y}$ nanostructured catalyst in a CO/He atmosphere at 400 °C, which helps to determine the mechanism of CO oxidation as well as the oxygen storage capacity of that catalyst.

2. Experimental

2.1. Catalyst preparation and characterization

The $Cu_{0.1}Ce_{0.9}O_{2-y}$ nanostructured catalyst was synthesized by a sol–gel method as described in [10]. After heat-treatment at 650 °C for 1 h in a flow of dry air, the catalyst powder was pelleted under a pressure of 100 bar for 1 min. These pellets were then crushed and sieved. The fraction of catalyst particles between 100 and 150 μm was used in kinetic experiments. Catalyst specific surface area was determined with a 5-point BET method from the N_2 adsorption isotherm measured with the Micrometrics TriStar 3000 gas adsorption analyzer. Structural changes of the catalyst were followed by X-ray powder diffraction (XRD) on a Philips PW1729 apparatus with a reflection technique.

2.2. Reactor system and analytical methods

The reactor consisted of a 4.6-mm-i.d. × 230-mm-long glass tube inserted into a heated aluminum block with o.d. 50 mm and length 155 mm. The reactor temperature was measured by a K-type thermocouple located in the middle of the aluminum block close to the reactor tube and regulated within the limits ±0.1 °C from the preset temperature by a PID temperature controller (Shimaden SR25).

During steady-state measurements the reactor temperature was varied in the interval between 45 and 155 °C. The mass of catalyst used in the experiments ranged from 37 to 251 mg. The catalyst was diluted with quartz beads (fraction in the range from 160 to 315 μm) with a minimum dilution ratio 1 : 1 by mass to about 15 mm packed bed length. The diluted catalyst was embedded with 10 mm of pure quartz beads on both sides. This ensures plug-flow and isothermal conditions within the bed. In a preliminary experiment, the catalyst bed temperature was measured by a glass-heated thermocouple placed axially into the reactor tube.

All reactant gases (O_2, H_2, CO_2, and He) were of purity N5 (Messer Slovenia), except CO, which had purity N2. A mixture of 4 vol.% CO in H_2 was prepared in a cylinder to ensure stable concentration of CO in the feed stream. A desired mixture of gases CO/H_2, H_2, O_2, and He was then prepared by adjusting the ratio of flows with calibrated mass flow controllers. In catalyst activity tests the CO concentration was always set to 0.01 bar and O_2 concentration was set to attain λ ($\lambda = 2P_{O_2}/P_{CO}$) values equal to 1 and 2.5, while the matrix was changed between pure He, pure H_2, or a mixture containing 0.5 bar H_2 and He as balance gas.

The gas mixtures for the kinetic experiments were prepared in such a way that the partial pressure of CO was varied between 0.001 and 0.025 bar and the partial pressure of O_2 was varied between 0.001 and 0.05 bar. The process parameter λ was varied between 0.2 and 40. Partial pressure of H_2 was always kept at 0.5 bar and He was used as a balance, yielding a total pressure of reaction gas mixture equal to 1 bar. In all steady-state experiments total gas flow rate was 100 mL/min.

Reactor inlet and outlet streams were analyzed by an HP 5890A gas chromatograph equipped with a temperature conductivity detector (TCD). Quantitative analysis of CO, CO_2, O_2, and H_2O in the H_2/He background was performed by column sequence reversal without backflush using two six-port Valco valves. CO_2 and H_2O were determined on a Porapak Q column (o.d. $1/8''$, length 3 m) while O_2 and CO were determined on a molecular sieve 13X column (o.d. $1/8''$, length 1.5 m). Helium was used as a carrier gas at a flow rate of 60 mL/min. The complete analysis could be obtained employing the following temperature program: 0–4 min isothermal at 85 °C; 4–12 min 85–130 °C with heating rate 70 °C/min. Methane formation was not detected under our experimental conditions. In order to control the steady state operation of the reactor, the reactor outlet stream was also continuously monitored for CO and CO_2 concentrations. This auxiliary measurement was performed by means of an IR gas analyzer (Rosemount, Binos-1000). The errors in the carbon mass balance were within ±0.3% by both means of analysis (GC and IR), which implies that no carbon deposits were formed on the catalyst surface. Nevertheless, the used catalysts were analyzed for total carbon (TC) using a Rosemount–Dohrmann DC-190 solid sample TC analyzer. No carbon-containing species were found on the catalyst after it had been used continuously for a week.

The CO conversion, X_{CO}, was calculated based on the CO_2 formation as follows:

$$X_{CO} = \frac{C_{CO_2}^{out}}{C_{CO}^{out} + C_{CO_2}^{out}} \times 100\%. \quad (1)$$

The O_2 conversion, X_{O_2}, was based on the oxygen consumption as follows:

$$X_{O_2} = \frac{C_{O_2}^{in} - C_{O_2}^{out}}{C_{O_2}^{in}} \times 100\%. \quad (2)$$

It was found that the reactor outlet stream contained no water at reaction temperatures of 90 °C and below, indicating 100% selectivity. When the temperature was increased above 90 °C, the first traces of water could be observed and the selectivity began to decline. When this was taking place, the selectivity, S, was calculated from the oxygen mass balance as follows:

$$S = \frac{0.5 \times C_{CO_2}^{out}}{C_{O_2}^{in} - C_{O_2}^{out}} \times 100\%. \quad (3)$$

The concentration steps in the transient regime were performed by the following setup: two feed sections converged at a four-way Valco valve, by which almost instant switching between feed sections could be achieved. Responses to the step-changes in the concentration of feed components were measured by a Leybold PGA 100 quadrupole mass spectrometer-QM. A signal was recorded and analyzed by a PC via RS232 connection.

In all transient experiments, total flow rate was set to 200 mL/min and reaction temperature was set to 400 °C. In these experiments, no oxygen and no hydrogen were present in the reactor feed.

2.3. Catalyst activity and reaction rate measurements

Prior to all experiments, the catalyst was pretreated *in situ* with a mixture of 20% O_2 in He (25 cm_3/min) at 400 °C for 30 min to clean the catalyst surface. Subsequently, the reactor was cooled down to 80 °C under the flow of the same gas mixture. After the catalyst was put on stream, we observed a fast initial catalyst deactivation over a period of about 8–16 h in all the experiments. Further deactivation was very slow. Therefore, an in situ lineout procedure prior to the kinetic experiments was developed. The conditions of the lineout procedure are listed in Table 1. Thus, each new sample of a catalyst was first pretreated in a 20% O_2/He mixture at 400 °C for 30 min and then the lineout procedure was employed. All the kinetic experiments were carried out during a subsequent period of maximum 12 h, and then a new sample of catalyst was used.

All steady-state kinetic experiments were performed when the reactor operated differentially. For this purpose, several experiments were performed to test the internal and external mass and heat transfer resistances of the catalyst as proposed by Dautzenberg [12]. For the catalyst pellets prepared as described in Section 2.1 it was found that there were no intraparticle mass transport limitations even if the catalyst fraction ranged from 400 to 500 μm. Tests on the external mass transport limitations were also performed. For total flow rates between 80 and 800 mL/min, no such limitations were found. By measuring the temperature inside the undiluted catalyst bed (200 mg of catalyst in the 10-mm length of catalyst bed), we found that the temperature of the undiluted catalyst bed increased linearly with CO conversion at a rate of 0.14 °C per 1% of CO conversion in the range

Table 1
Experimental conditions for the catalyst lineout procedure

Temperature (°C)	80
Total gas flow rate (mL/min)	100
Total pressure (bar)	1
Feed partial pressures (bar)	
Carbon monoxide	0.01
Oxygen	0.0125
Hydrogen	0.5
Helium	0.4775
Time on stream (h)	16

$0 < X_{CO} < 70\%$. In kinetic experiments, the CO conversion was adjusted by the catalyst loading and kept between 5 and 10%. Lower conversions were not used in order to obtain accurate enough analyses. When the conversion was 10% the temperature increased by at most 1.4 °C. In order to ensure isothermal operation of the bed, the catalyst was diluted further by quartz beads, as described above. At this point we concluded that rigorous enough conditions were fulfilled to assume that there were no heat transfer limitations. The results of all the above tests gave us confidence that the reactor was operating under isothermal and differential conditions.

The reaction rate was calculated from CO_2 production in [mol/g_{cat} s] as

$$\text{Rate} = \dot{n}_{tot} \cdot y_{CO_2} / W_{cat}, \quad (4)$$

where $\dot{n}_{tot}$ is the total molar gas flow rate (mol/s), y_{CO_2} is the molar fraction of CO_2 in the product gas stream, and W_{cat} is the mass of the catalyst (g).

The reducibility of the catalyst was measured by the transient experiments. In this case, the catalyst was first pretreated with the O_2/He mixture at 400 °C and then the lineout procedure was employed to produce better repeatability of the experiments. When the lineout procedure was over, the catalyst was completely reoxidized again in a flow of O_2/He mixture under the same conditions as in the initial pretreatment. When the reoxidation was over, the temperature was left at 400 °C, the flow of oxygen was stopped, and the flow rate of He was adjusted to 200 mL/min. The reactor was purged with pure He for 10 min in order to desorb the remaining physisorbed oxygen from the catalyst surface. In the second feed section, a mixture of CO/He with a partial pressure of CO equal to 0.01 bar was prepared and the flow rate of the latter mixture was also set to 200 mL/min. Then the switch from He to CO/He feed sections was performed by means of a four-way valve. This was equal to a CO concentration step change over completely oxidized catalyst.

Transient experiments were performed in the isothermal mode of operation, since the maximum temperature jump after performing the concentration step was measured to be 1.5 °C. In this case, though, the catalyst was diluted at least six times by mass with quartz beads.

3. Results

3.1. The stability of $Cu_{0.1}Ce_{0.9}O_{2-y}$ oxidation catalysts under medium and severe reducing conditions

Figure 1 shows the deactivation curves for selective CO oxidation over a $Cu_{0.1}Ce_{0.9}O_{2-y}$ nanostructured catalyst in the reducing atmosphere. The catalyst samples were only pretreated in an O_2/He mixture at 400 °C and then cooled to reaction temperature. For each of the three experiments 100 mg of catalyst was used. Partial pressures of reactants and total flow rate were the same as in the lineout procedure. Two different catalyst samples, denoted by △ and □, took similar deactivation paths when the reactor temperature was set to 80 °C, the working temperature of the PEM fuel cell. The catalysts exhibited around 40% CO conversion when put on stream, but after several hours they stabilized at 30%, indicating fast initial deactivation and afterward very stable catalyst activity. When the reaction temperature was set to 155 °C (sample denoted by ○), no deactivation was observed. The reason for this lies in the fact that 100 mg of the catalyst at a temperature of 155 °C is far enough to attain 100% CO conversion for the flow rates and partial pressures of reactants as stated above, regardless of the fast initial deactivation, which is certainly present. The latter temperature is in fact above the working range of the PEM fuel cell, but in this case it was used to show the deactivation behavior of the catalyst at the highest temperatures used in the present work.

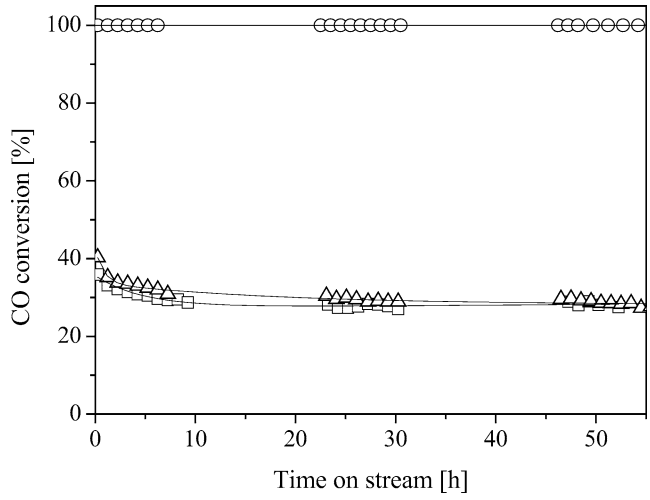

Fig. 1. Deactivation curves for the selective CO oxidation over two samples of $Cu_{0.1}Ce_{0.9}O_{2-y}$ nanostructured catalyst at a reaction temperature of 80 °C (denoted by △ and □) and one sample deactivated at 155 °C (denoted by ○). Total gas flow rate and partial pressures of reactants were the same as in the lineout procedure (Table 1). Catalyst samples were pretreated in O_2/He at 400 °C. $W_{cat} = 100$ mg.

Table 2 presents BET surface area measurements and Fig. 2 presents XRD patterns of fresh catalyst and of two different samples of catalyst that were deactivated for 48 h at 80 and 155 °C, respectively. Neither from BET surface area measurements nor from XRD patterns could deformations of the bulk catalyst structure be detected after 48 h on

Table 2
BET specific surface areas of fresh sample and two different samples initially pre-treated and then deactivated for 48 h at two different temperatures

Treatment temperature (°C)	BET surface area (m^2/g)
Fresh catalyst	22.7
80	21.7
155	22.0

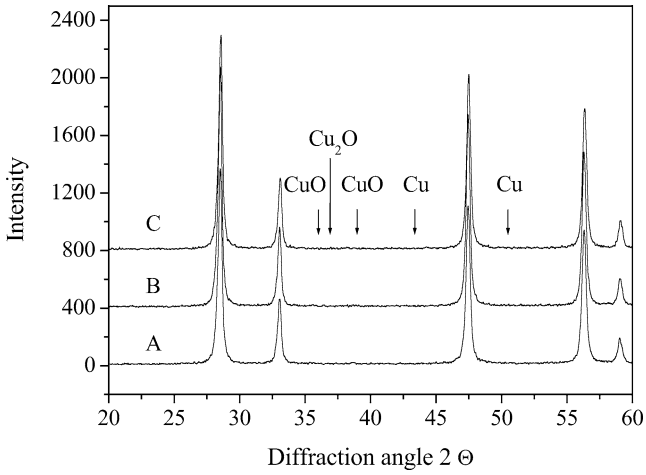

Fig. 2. XRD patterns of a fresh $Cu_{0.1}Ce_{0.9}O_{2-y}$ nanostructured catalyst and of two samples subjected to initial pretreatment, which was followed by 48 h deactivation at different temperatures. Positions of expected diffraction peaks of different copper-containing phases are denoted by arrows: (A) fresh catalyst; (B) deactivation temperature 80 °C; (C) deactivation temperature 155 °C. In the deactivation processes the same flow rates and partial pressures of reactants as in the lineout procedure were used.

stream. Before BET and XRD analysis of the sample that was deactivated at 155 °C, CO conversion at 80 °C was measured for a reference to be 30%, so no difference was found if the catalyst sample was deactivated at 80 °C or at 155 °C.

In order to find which type of deactivation of the $Cu_{0.1}Ce_{0.9}O_{2-y}$ nanostructured catalyst is taking place, another experiment similar to that presented in Fig. 1 was employed. This time, we performed the deactivation experiment at a temperature of 80 °C, but for 172 h. Fast initial deactivation was observed from the time the catalyst was put on stream, since CO conversion dropped from about 40 to 30% over the first several hours. Further deactivation was very slow, since the catalyst exhibited a conversion of around 25% after 172 h. Then we tried to regenerate the catalyst. We stopped the reaction and treated the catalyst in a flow of 20 vol.% O_2 in He at 400 °C for 30 min to desorb CO, CO_2, and eventually H_2O from the surface. Then the reactor was cooled to 80 °C and the reaction of selective CO oxidation was started again. After the stabilization of flows, the conversion was the same as before the applied regeneration procedure (25%). From this it can be concluded that the deactivation process is irreversible.

The stability of the catalyst under transient redox cycling was almost unchanged, since the lineout procedure employed before the first redox cycle encompassed fast initial deactivation of the catalyst. In fact, the catalyst performed an 18.5% CO conversion (catalyst load of 65 mg) after the lineout procedure, while it was measured to be 18.0% after 15 consecutive redox cycles (heating to 400 °C in a flow of O_2/He, several minutes of CO reduction at temperatures of up to 400 °C, followed by reoxidation in a flow of O_2/He again at 400 °C) when put back to lineout conditions.

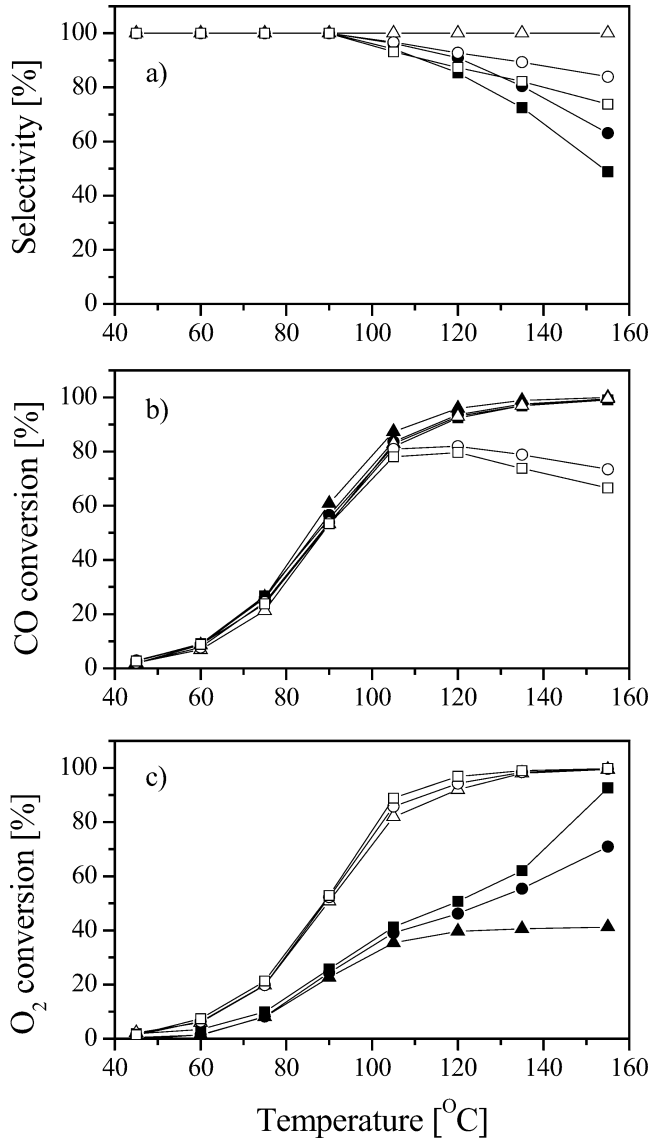

Fig. 3. Selectivity (a) and conversions of CO (b) and O_2 (c) obtained over the $Cu_{0.1}Ce_{0.9}O_{2-y}$ catalyst as a function of temperature, λ value, and H_2 presence in the reactor feed. (■, □) CO, O_2, and H_2 in the reactor feed, no He; (●, ○) CO, O_2, 50% H_2, He balance gas; (▲, △) CO, O_2, and He in the reactor feed, no H_2. Full symbols denote $\lambda = 2.5$, while empty symbols denote $\lambda = 1$. In all experiments $P_{CO} = 0.01$ bar, total pressure is equal to 1 bar, $W_{cat} = 100$ mg, $\dot{n}_{tot} = 100$ mL/min.

3.2. The catalyst activity and selectivity as functions of reaction temperature and feed gas composition

Figure 3 shows the conversion of CO and O_2, as well as the selectivity obtained in the CO oxidation reaction over the nanostructured $Cu_{0.1}Ce_{0.9}O_{2-y}$ catalyst. Regarding the selectivity of the catalyst, it is obvious that it stays at 100% in all temperature ranges for the case where there is no H_2 present in the reactor feed. However, when the reactor feed contains H_2, the selectivity starts decreasing at temperatures higher than 90 °C. If we examine the effect of hydrogen content on the selectivity, it can be noted that above 90 °C the selectivity is always less in the case where only oxygen,

carbon monoxide, and hydrogen are present in the reactor feed compared to the case where almost 50 vol.% of He dilutes the hydrogen (full squares compared to full circles as well as empty squares compared to empty circles). This is normal, because in the previous case the H_2 partial pressure (potential to form water) is higher compared to the latter case.

Besides the hydrogen partial pressure in the feed, the O_2/CO stoichiometric ratio also influences the selectivity of the catalyst. If oxygen is present in excess in the reactor feed ($\lambda = 2.5$), more oxygen is available for the hydrogen oxidation reaction to form water if compared to the case where those two reactants are present in a stoichiometric ratio equal to one ($\lambda = 1$). This is clear if we compare full and open circles as well as full and open squares from Fig. 3a.

The conversion of carbon monoxide is connected to both hydrogen and oxygen partial pressures in the reactor feed gas. At temperatures of up to 90 °C, where no side reaction of hydrogen oxidation occurs, the CO conversion is independent of hydrogen partial pressure, while there is a very week dependence on oxygen partial pressure (empty symbols are a little bit lower than full ones on Fig. 3b) in that temperature region. In Section 3.3 we will study the influence of O_2 partial pressure on the reaction rate in more detail. If the temperature is raised above 90 °C, water is also formed. In that case the CO conversion becomes much more dependent on oxygen and hydrogen partial pressures. These dependences are interconnected with each other and subordinate to the water formation reaction. If the stoichiometric ratio of oxygen ($\lambda = 1$) is fed to the reactor in the presence of hydrogen, the CO conversion reaches its maximum value of around 80% at a temperature of 105 °C. At higher temperatures, the CO conversion curve lowers again. Because more and more water is formed when temperature increases, less and less oxygen remains available for the CO oxidation reaction. There is only a small difference in the CO conversion if the hydrogen partial pressure is 0.5 or 0.985 bar, as depicted by open circles and squares, respectively, in Fig. 3b. If there is no hydrogen present in the reactor feed, CO conversion reaches 100%.

When oxygen is present in excess in the reactor feed ($\lambda = 2.5$), the CO conversion curve does not fall from 100% even at a reaction temperature of 155 °C. At that temperature, there is still around 10 or 30% (full squares and full circles, respectively, in Fig. 3c) oxygen left in the system. That is enough to attain 100% CO conversion plus the formation of the corresponding amount of water. It seems that the conversion of carbon monoxide is literally independent of hydrogen partial pressure in all temperature regions as long as there is enough oxygen fed to the reactor. Only the amount of water formation is dependent on hydrogen partial pressure, as seen from closed symbols from Figs. 3a and 3c, which is a side reaction.

In the case of $\lambda = 2.5$, it is interesting to follow O_2 conversion curves. O_2 conversion is independent of H_2 partial pressure up to a temperature of 90 °C as depicted in Fig. 3c, full symbols. In the case where there is no H_2 present in the system, the O_2 conversion curve is very similar to the CO conversion curve (full triangles). It reaches 40% at high temperatures, as predicted from stoichiometry, i.e., $100\%/\lambda$. The O_2 conversion curve has a *single-S shape*. In the case where hydrogen is present in the reactor feed, it takes off again above 40% because of the water formation reaction at the reaction temperature of 105 °C and starts to approach 100%. It has a characteristic *double-S shape*. In the case $\lambda = 1$, the oxygen conversion reaches 100% faster in the case where there is also hydrogen present in the reactor feed, because in that case it is consumed both for the CO and for the H_2 oxidation reaction.

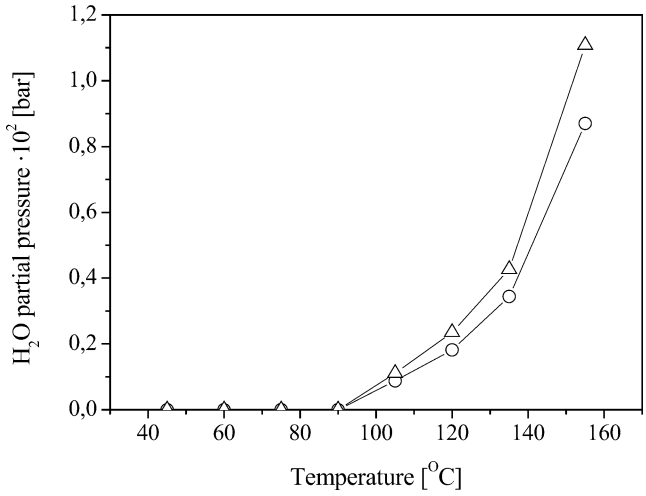

Fig. 4. Partial pressure of water in the reactor effluent stream; (○) $P_{O_2} = 0.02$ bar, $P_{H_2} = 0.98$ bar, no CO, no He; (△) $P_{O_2} = 0.02$ bar, $P_{CO} = 0.01$ bar, $P_{H_2} = 0.97$ bar, no He; $W_{Cat} = 100$ mg, $\dot{n}_{tot} = 100$ mL/min.

As a reference, we also studied the hydrogen oxidation reaction under conditions where CO was present and also in the case where it was not present in the feed gas. In Fig. 4 the water partial pressures in the reactor effluent stream are represented as a function of temperature and feed gas composition. The reactor feed for the run denoted by circles contained only 0.02 bar O_2 and 0.98 bar hydrogen, while in the case denoted by triangles the reactor feed consisted of 0.02 bar O_2, 0.01 bar CO, and 0.97 bar H_2. In both cases the water formation started at a reaction temperature of 105 °C. It is interesting to notice that H_2O partial pressure is around 15–20% higher in the case where the reactor feed also contains CO than in the case where it is absent. In the case of the presence of CO in the reactor feed, it must be mentioned that the $Cu_{0.1}Ce_{0.9}O_{2-y}$ nanostructured catalyst copes with much higher oxygen conversions. At a temperature of 155 °C, for instance, oxygen conversion is 25% for the complete CO oxidation reaction plus 27% for the H_2 oxidation reaction, yielding a total O_2 conversion of 52%. On the other hand, in the case where no CO was present in the reactor feed, oxygen conversion was

merely around 22% for the H_2 oxidation reaction at 155 °C. This was found to be a general behavior for the $O_2 + H_2$ vs $O_2 + CO + H_2$ reactions over the $Cu_{0.1}Ce_{0.9}O_{2-y}$ nanostructured catalyst regardless of changes of oxygen and carbon monoxide partial pressures in the reactor feed.

There exist a large set of thermodynamically allowed equilibrium reactions in the case of selective oxidation of CO in excess hydrogen. They are discussed in more detail in the Discussion (Section 4.1). At this point, one could propose that more water was found in the case where CO was present in the reactor feed because of the reverse water gas-shift (WGS) reaction—one among the possible reactions in that set. If we check the thermodynamic equilibrium constant for the forward WGS reaction we find that it is 4.2×10^3 at 90 °C and 4.9×10^2 at 155 °C. In spite of this we still tested the catalyst on the reverse WGS reaction by feeding the reactor with a mixture consisting of 0.01 bar CO_2 and 0.99 bar H_2. We did not find any CO in the reactor effluent gas in the temperature range from 90 to 155 °C. The conclusion from this could be that CO promotes the water formation reaction.

Avgouropoulos et al. [6] recently studied the addition of CO_2 and H_2O in the feed gas over a similar nanostructured $Cu_{0.1}Ce_{0.9}O_{2-y}$ catalyst prepared by a coprecipitation method. They reported that the addition of 15% CO_2 in the feed gas decreases the activity of the catalyst. Under these conditions the same values of activity and selectivity were obtained at 15–35 °C higher temperatures. The addition of 10% H_2O in the feed shifted the activity and selectivity curves to 20–40 °C higher temperatures with respect to the curves where only CO, O_2, H_2, and He were used in the feed.

3.3. Kinetic results

Figure 5 shows variation in the rates of carbon monoxide selective oxidation in a 50% H_2 atmosphere under different reaction conditions. The temperature in these kinetic measurements was varied in the range 48–90 °C where the nanostructured $Cu_{0.1}Ce_{0.9}O_{2-y}$ catalyst is 100% selective; i.e., no water is present in the reactor effluent stream. The reaction rates increase nonlinearly with both CO and O_2 partial pressures. However, in all these experiments the observed rates never leveled off with increasing P_{CO} or P_{O_2}. Comparing Figs. 5a and 5b one can see that the reaction rate increases more steeply with P_{O_2} than with P_{CO} at low partial pressures, but at higher partial pressures the reaction rate is less sensitive to the increase of P_{O_2} than to the increase of P_{CO}. Because no maximum in the reaction rate was found when either CO or O_2 partial pressures were varied, it seems that those two reactants do not adsorb competitively on the surface. Apart from this, the reaction rate has the shape of a Langmuir isotherm when CO partial pressure is varied, while when O_2 partial pressure is varied it is completely different (Fig. 5). This implies that neither a classical Eley–Rideal nor the Langmuir–Hinshelwood kinetics is present in

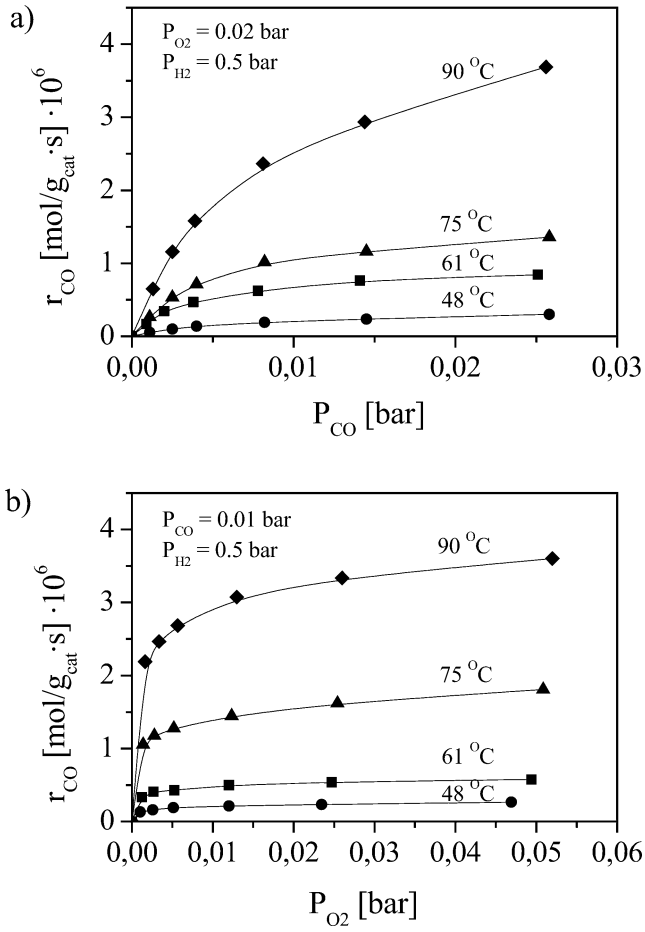

Fig. 5. Variation of the selective CO oxidation rate in excess hydrogen over the nanostructured $Cu_{0.1}Ce_{0.9}O_{2-y}$ catalyst with partial pressures of reactants and with the reaction temperature. Mass of the catalyst was varied in order to assure differential conditions in the reactor. (a) Variation of CO oxidation rate with partial pressure of CO and temperature at $P_{O_2} = 0.02$ bar. (b) Variation of CO oxidation rate with partial pressure of O_2 and temperature at $P_{CO} = 0.01$ bar. Partial pressure of H_2 was always equal to 0.5 bar and He was used as a balance gas. Mass of catalyst varied as explained in text; $\dot{n}_{tot} = 100$ mL/min.

the CO selective oxidation over the $Cu_{0.1}Ce_{0.9}O_{2-y}$ nanostructured catalyst.

It is now widely accepted that both CO and H_2 oxidation reactions involving molecular oxygen over metal oxide catalysts proceed by a redox mechanism [13,14]. In particular, the CO oxidation reaction over the nanostructured $Cu_xCe_{1-x}O_{2-y}$ oxide catalysts was confirmed to obey this type of reaction [15–17]. The oxidation of H_2 over the $CeCu_xO_y$ mixed oxide is subject to the same redox mechanism [18].

Such a redox reaction can be described by the following two-step reaction:

$$\text{Cat–O} + \text{Red} \rightarrow \text{Cat} + \text{Red–O},$$

$$\text{Cat} + \text{Ox–O} \rightarrow \text{Cat–O} + \text{Ox}.$$

The first step in this reaction mechanism is the catalyst reduction. Cat–O represents oxidized catalyst, which is

attacked by a reductant (Red). Catalyst itself undergoes reduction, while the reductant is oxidized. The second step represents reoxidation of the catalyst by the oxidant (Ox–O), which donates an oxygen atom to the catalyst while it reduces itself.

The kinetics of selective CO oxidation over the $Cu_{0.1}Ce_{0.9}O_{2-y}$ nanostructured catalyst can be well described by employing the Mars and van Krevelen type of kinetic equation derived on the basis of a redox mechanism [19]

$$r_{CO} = \frac{k_{CO} k_{O_2} P_{CO} P_{O_2}^n}{0.5 \cdot k_{CO} P_{CO} + k_{O_2} P_{O_2}^n}, \quad (5)$$

$$k_{CO} = A_{CO} \cdot \exp(-E_{a,CO}/RT), \quad (6)$$

$$k_{O_2} = A_{O_2} \cdot \exp(-E_{a,O_2}/RT). \quad (7)$$

The parameters k_{CO} and k_{O_2} in Eqs. (6) and (7) are taken to be the reaction rate constants for the reduction of surface by CO and reoxidation of it by O_2. The parameters k_{CO}, k_{O_2}, and n at one temperature were obtained by fitting experimental values of P_{CO}, P_{O_2}, and reaction rate with Eq. (5). Since the parameter n was floating in the range $n = 0.2 \pm 0.05$ over the four different temperatures, the final values of parameters k_{CO} and k_{O_2} at each temperature were calculated with a fixed value of n equal to 0.2. It should be mentioned, however, that for each point representing k_{CO}, k_{O_2} and n at a particular temperature, two different samples of a fresh catalyst with their own deactivation behavior were used (one sample to determine r_{CO} vs P_{CO} and the other sample to determine r_{CO} vs P_{O_2} at a particular temperature). The reason for this is in fact that in order to maintain the CO conversion in the range 5–10%, it was necessary to take an appropriate mass of catalyst for the particular experimental conditions. This yielded eight different sample sets of catalysts.

The same data can also be regressed almost equally well by the model of Liu and Flytzani-Stephanopoulos [20]. The equations that describe this model are as follows:

$$r_{CO} = \frac{k_L K_L P_{CO} P_{O_2}^m}{1 + K_L P_{CO}},$$

$$k_L = A_L \cdot \exp(-E_{a,L}/RT),$$

$$K_L = B_L \cdot \exp(Q/RT).$$

The parameters k_L and K_L in the former model can be taken as the surface reaction rate constant and CO adsorption equilibrium constant, respectively. When the data in Fig. 5b are replotted on a log–log scale they give almost straight lines with a slope (exponent m) of 0.15 ± 0.025 with a correlation coefficient of 0.986 or better.

Arrhenius plots of the constants k_{CO}, k_{O_2}, k_L, and K_L obtained over the whole temperature interval studied are shown on Fig. 6. The values of preexponential factors, apparent activation energies and heat of CO adsorption obtained from the Mars and van Krevelen model, as well as from the Liu and Flytzani-Stephanopoulos model, are given in Table 3.

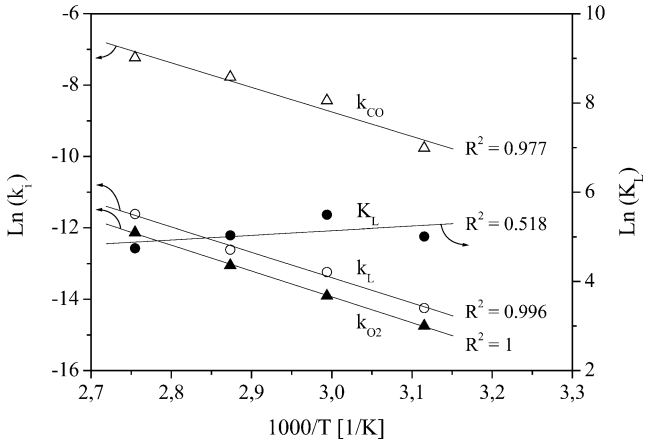

Fig. 6. Arrhenius plots of the rate constants for the selective CO oxidation in excess of hydrogen over the $Cu_{0.1}Ce_{0.9}O_{2-y}$ nanostructured catalyst; (△) k_{CO}, (▲) k_{O_2}, both Mars and van Krevelen model; (○) k_L, (●) K_L, both Liu and Flytzani-Stephanopoulos model.

Figure 7 represents the calculated vs experimental values of reaction rates for both Mars and van Krevelen and for Liu and Flytzani-Stephanopoulos models for the selective CO oxidation in excess of hydrogen over the $Cu_{0.1}Ce_{0.9}O_{2-y}$ nanostructured catalyst. From that figure one can see that most of the scatter of data represents the use of eight different catalyst samples; the data obtained over one catalyst sample lie on an almost straight line. In order to discriminate between the two models, for each of the eight sets of experimental data from Figs. 7a and 7b its own linear least squares fit was calculated. The correlation coefficients of the eight sets from both models came to 0.983 or better. The average value of slopes and the average value of sections on the y-axes from Figs. 7a and 7b with the corresponding standard deviations were calculated for each experimental set of data. Using the standard T_n-test [21] it was found that there were no outliers among sets of data for the 95% confidence limit either for the Mars and van Krevelen model or for the Liu and Flytzani-Stephanopoulos model. The comparison of an experimental mean of slopes and experimental mean of sections on the y-axes with the true values (equal to 1 and 0, from Figs. 7a and 7b, respectively) using the standard t-test [21] showed that no bias is present in our experiments for the 95% confidence level.

Table 3
Calculated values of kinetic parameters obtained from the Mars and van Krevelen model as well as from Liu and Flytzani-Stephanopoulos model for selective CO oxidation over the $Cu_{0.1}Ce_{0.9}O_{2-y}$ nanostructured catalyst

Mars and van Krevelen model		Liu and Flytzani-Stephanopoulos model	
A_{CO} (mol/g_{cat} s bar)	1.44×10^5	A_L (mol/g_{cat} s bar^m)	2.64×10^3
$E_{a,CO}$ (J/mol)	5.72×10^4	$E_{a,L}$ (J/mol)	5.9×10^4
A_{O_2} (mol/g_{cat} s bar^n)	2.39×10^3	B_L (1/bar)	7.53×10^0
E_{a,O_2} (J/mol)	6.02×10^4	Q (J/mol)	8.7×10^3
n (/)	0.2 ± 0.05	m (/)	0.15 ± 0.025

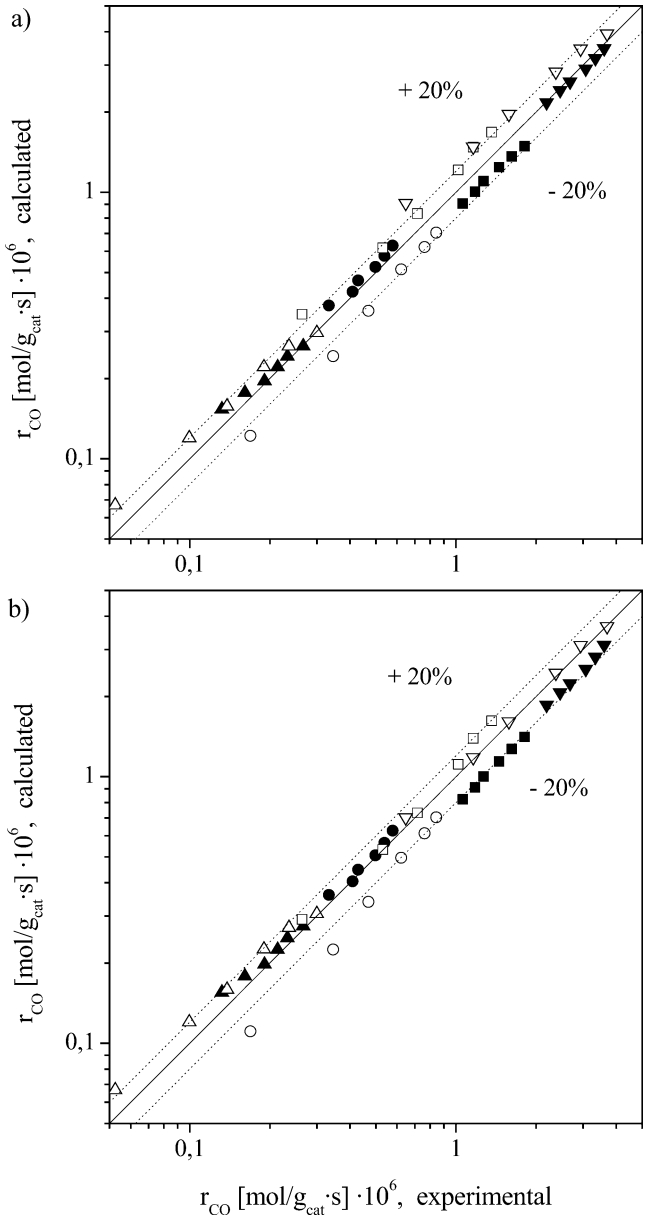

Fig. 7. Parity plots of reaction rates for the selective CO oxidation in excess of hydrogen over the $Cu_{0.1}Ce_{0.9}O_{2-y}$ nanostructured catalyst in the 100% selectivity region; (a) Mars and van Krevelen model; (b) Liu and Flytzani-Stephanopoulos model. (▲, △) $T = 48$ °C; (●, ○) $T = 61$ °C; (■, □) $T = 75$ °C; (▼, ▽) $T = 90$ °C. Full symbols denote variation in oxygen, while empty symbols denote variation in carbon monoxide partial pressure.

Discrimination between the two models on the basis of the scatter between experimental and calculated values (which is based on sum of squares of relative errors) is also impossible, for it is approximately the same for both models. However, the model proposed by Liu and Flytzani-Stephanopoulos gives a heat of adsorption of 8.7 kJ/mol with a correlation coefficient equal to 0.518 (Fig. 6). It must be noted, though, that such a poor correlation coefficient does not originate from the scatter in the data but from the nonlinearity in the Arrhenius plot. If we recall that no physical transport resistances were observed in our experimental set-up, such nonlinearity in the Arrhenius plot cannot be explained. On the other end, if we simply omit the last point from the calculation of the heat of CO adsorption as a supposedly bad measurement (Fig. 6), the heat of CO adsorption comes to 25.9 kJ/mol while the preexponential coefficient B_L comes to 2.1×10^{-2} 1/bar (compare to the values from Table 2). It must be mentioned that the last two values are very close to the values reported in the article by Liu et al. [20] for the $Cu_{0.15}[Ce(La)]_{0.85}O_y$ catalyst prepared by a coprecipitation method and calcined at 650 °C, regarding complete oxidation of carbon monoxide without the presence of hydrogen. In that article, the heat of CO adsorption was reported to be 27.9 kJ/mol, while the preexponential factor B_L was equal to 6.47×10^{-3} 1/bar. But, if we insert Q and B_L equal to 25.9 kJ/mol and 2.1×10^{-2} 1/bar, respectively, into the model of Liu and Flytzani-Stephanopoulos, we get the sum of squares of relative errors a little less than three times higher than obtained from Fig. 7a or 7b, with relative errors deviating severely in the low-temperature region.

3.4. Reduction of $Cu_{0.1}Ce_{0.9}O_{2-y}$ nanostructured catalyst by carbon monoxide

In order to find the type of oxygen (physisorbed, surface lattice or crystalline bulk) that reacts in the CO oxidation reaction, isothermal concentration step changes of feed gas of type He → CO/He were used. Figure 8 shows the response of a fully oxidized catalyst to such a concentration step change at a temperature of 400 °C. Irrespective of the fact that no oxygen was fed to the reactor, and a relatively high (200 mL/min) feed flow rate and low mass of the catalyst (65 mg) were used; the CO conver-

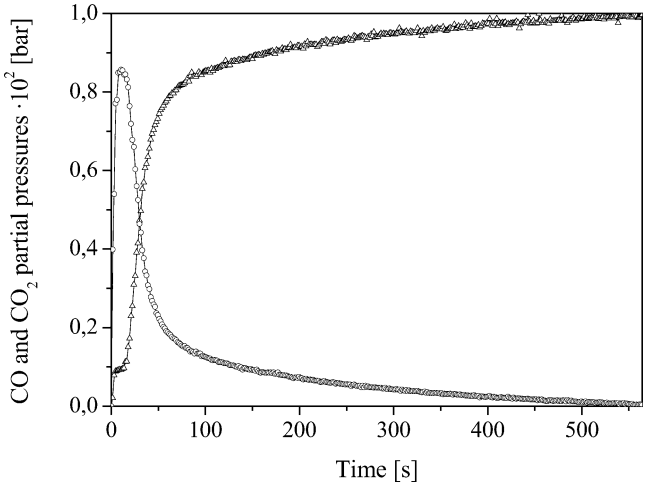

Fig. 8. Response to an He → CO/He concentration step over fully oxidized catalyst. Partial pressures of CO (△) and CO_2 (○) are measured at the outlet of the reactor. Initial partial pressures: $P_{He} = 1$ bar; partial pressures after the concentration step change: $P_{CO} = 0.01$ bar, $P_{He} = 0.99$ bar. Conditions: $T = 400$ °C, $W_{cat} = 65$ mg, $\dot{n}_{tot} = 200$ mL/min.

sion reached 85%. After the peak conversion, the CO_2 signal starts falling. After 3 min, however, the catalyst still exhibits approximately 10% CO conversion and after 5 min, it drops to 5%. Available oxygen for the CO → CO_2 reaction is depleted in a little less than 10 min, when no evolution of CO_2 was detected by the mass spectrometer.

The amount of oxygen that was consumed in the CO → CO_2 reaction at a temperature of 400 °C was estimated. This was done by integrating the area under the CO_2 curve (or, alternatively, above the CO curve) from Fig. 8 and multiplying by the gas flow rate (200 mL/min). The numerical integration was preformed using Simpson's formula over all data points. Taking into consideration the stoichiometry, 4.0×10^{-5} mol O_2 was consumed in the carbon monoxide oxidation reaction.

The question now is what is the origin of the oxygen that was consumed in the CO oxidation reaction. The first, most straightforward idea is that the oxygen comes from the physisorbed layer. We estimated the amount of physisorbed oxygen needed to cover one complete monolayer of catalyst surface. The effective area occupied by one O_2 molecule was estimated to be 0.136 nm^2 (14.7 at. O/nm^2) by using the Emmett and Brunauer formula [22]. When this was compared to the BET specific surface area of the $Cu_{0.1}Ce_{0.9}O_{2-y}$ nanostructured catalyst (Table 2), 1.75×10^{-5} mol O_2 was calculated to be enough to cover one complete physisorbed monolayer of 65 mg catalyst surface. In other words, the evaluated amount of O_2 that was consumed in the CO → CO_2 reaction would be enough to cover 2.3 monolayers of physisorbed oxygen. The assumption that the oxygen needed for the CO oxidation reaction comes only from the physisorbed layer is even less likely to be valid since before the CO step change was performed, the catalyst was purged for 10 min in pure He at the reaction temperature to strip off the physisorbed oxygen.

The next possible oxygen source is surface oxygen from the catalyst lattice. First, we assume that only oxygen from the copper oxide of the $Cu_{0.1}Ce_{0.9}O_{2-y}$ nanostructured catalyst is involved in the CO oxidation reaction. From XRD patterns of the $Cu_{0.1}Ce_{0.9}O_{2-y}$ nanostructured catalyst no copper-containing phase was found (Fig. 2). One possible explanation of this could be that the copper oxide is present as an amorphous layer over the ceria support surface. Now, let us assume that all copper atoms are involved in the reaction. It can be calculated that 65 mg of $Cu_{0.1}Ce_{0.9}O_{2-y}$ nanostructured catalyst contains 4.0×10^{-5} mol of copper. If this copper existed initially as Cu^{2+} (first extreme) and all of it was reduced at 400 °C to Cu^0 (the other extreme), only 50% (4.0×10^{-5} mol) of CO would be consumed in this case. Now, if we suppose that the surface density of oxygen atoms in ceria phase is 14.7 at. O/nm^2 as calculated from the physisorption model, a little more than 1 additional monolayer of oxygen is extracted from the ceria phase. However, oxygen chemisorbed as oxide ion occupies substantially more room than physisorbed oxygen. Ceria has a face-centered cubic crystal structure. It can be calculated that the surface density of the outer ceria cation monolayer in the most likely exposed faces of ceria, the (111) and (110) planes, is 7.9 and 4.85 Ce/nm^2, respectively. If we recalculate the number of cerium atoms in one monolayer, we get the result that 1.5×10^{-5} mol cerium cations are present in one monolayer if 50% of Ce cations are found in the (111) exposed plane and the rest in the (110) exposed plane. Now, if we take into consideration the stoichiometry, more than 5.3 monolayers of oxygen atoms would be consumed from the ceria phase. The latter number, however, would be reduced in practice since the actual area of cerium atoms is not exactly known. There is also a possibility of micropores in the catalyst structure that are BET-invisible, so the actual number of Ce atoms in one monolayer could be higher than estimated.

To conclude this speculative approach, it can be estimated that the reduction of the $Cu_{0.1}Ce_{0.9}O_{2-y}$ nanostructured catalyst by carbon monoxide at 400 °C is 2 to 6 monolayers deep (1 monolayer for the Cu phase and 1 to 5 monolayers for the Ce phase). At lower temperatures, however, the amount of oxygen that is extracted from the subsurface ceria crystal lattice is certainly lower. We have observed the same pattern of CO and CO_2 responses as presented in Fig. 8 (an instant CO_2 peak followed by long tailing) at temperatures down to 50 °C. At a temperature of 50 °C, however, a much lower peak was found and a tailing was finished in about 7 min. It is hardly possible that appreciable amounts of subsurface lattice oxygen are extracted by CO reduction at this low temperature. Nevertheless, it is important to notice that there is not (only) physisorbed oxygen involved in the CO oxidation reaction, but also surface crystal lattice oxygen (mainly at lower temperatures) and also subsurface (bulk) crystal lattice oxygen (joins in at higher temperatures) take part in the CO oxidation reaction. The ratios between the types of oxygen species involved changes with catalyst composition, feed gas composition, and reaction temperature.

It was found that CeO_2 could formally be written as $CeO_{1.83}$ in the H_2 and CO reducing atmosphere [23,24], designating the oxygen storage capacity to be 0.17. In the last experiments, however, the latter values were obtained for temperature programmed reduction (TPR) experiments up to 600 °C with samples having a specific surface area considerably higher than that for the samples used in the present study. Since the catalyst sample (CeO_2) in the references [23,24] had a BET specific surface area around 115 m^2/g compared to 22 m^2/g of $Cu_{0.1}Ce_{0.9}O_{2-y}$ sample in the present study, it can be calculated that much deeper reduction was achieved by CO reduction of the $Cu_{0.1}Ce_{0.9}O_{2-y}$ nanostructured catalyst (2–6 monolayers) when compared to H_2 and CO reduction of the CeO_2 catalyst (1–2 monolayers).

4. Discussion

4.1. General considerations regarding selective CO oxidation in the presence of excess hydrogen

Taking into account the composition of the gas mixture at the outlet of the low-temperature water gas-shift reactor, one can conclude that there are quite a number of thermodynamically allowed reactions. Even in our case, when the gas feed into PROX reactor does not contain CO_2 and H_2O, one has to consider the following set of thermodynamic equilibria:

$$CO + \tfrac{1}{2}O_2 \Leftrightarrow CO_2, \quad (8)$$

$$H_2 + \tfrac{1}{2}O_2 \Leftrightarrow H_2O, \quad (9)$$

$$CO + H_2O \Leftrightarrow CO_2 + H_2, \quad (10)$$

$$2CO \Leftrightarrow C + CO_2, \quad (11)$$

$$CO + 3H_2 \Leftrightarrow CH_4 + H_2O, \quad (12)$$

$$CO_2 + 4H_2 \Leftrightarrow CH_4 + 2H_2O. \quad (13)$$

Reaction (11) is completely unwanted, because it reduces the activity of a catalyst by coking. Reactions (9), (12), and (13) are also unwanted, because they reduce the selectivity of a catalyst. Consequently, a catalyst with a good selectivity will promote reaction (8) or (10) at the expense of reactions (9), (12), and (13). Thermodynamic equilibrium constant of the water gas-shift reaction (WGSR) (10) is at least 25 orders of magnitude lower than the thermodynamic equilibrium constants of CO and H_2 oxidation reactions in the temperature range of performed kinetic experiments. It was experimentally observed that the WGSR does not proceed to an appreciable extent over the Cu–Ce(La)O_x [25] and CuO/Al_2O_3–CeO_x [7] catalyst at temperatures below 150 °C and at high GHSV ($> 80{,}000\ h^{-1}$). The results from the present study confirm also that no reverse WGS reaction is observed over the $Cu_{0.1}Ce_{0.9}O_{2-y}$ nanostructured catalyst at temperatures below 155 °C. Both methanation reactions (12) and (13) have extremely low values of the thermodynamic equilibrium constant (on the order of 10^{-20}) at these low temperatures and we did not observe even traces of methane in our kinetic experiments. The formation of carbon, reaction (11) (Boudouard equilibrium), is favored at low temperatures, but again the thermodynamic equilibrium constant is at least 20 orders of magnitude lower than the thermodynamic equilibrium constants of the CO and H_2 oxidation reactions in this temperature interval. From the thermodynamic point of view there are no restrictions for the oxidation of CO to proceed with 100% selectivity in excess of H_2 if both oxidation reactions proceed near equilibrium.

4.2. Synergistic effects of copper and ceria in the $Cu_{0.1}Ce_{0.9}O_{2-y}$ nanostructured catalyst

It was found that the $Cu_xCe_{1-x}O_{2-y}$ catalyst, depending on the method of preparation (impregnation, coprecipitation, or sol–gel) and on the quantity of copper added (x), exhibits the presence of both distinct crystallographic phases (CuO and CeO_2) at higher values of x and higher heat-treatment temperatures, while at lower values of x (less than 0.1 for samples prepared by coprecipitation and less than 0.2 for samples prepared by the sol–gel route) and lower heat-treatment temperatures (less than 873 K) it exhibits only the presence of CeO_2 with the fluorite structure. Up to 20% of copper oxide in the sol–gel prepared samples is thus X-ray amorphous (see Fig. 2). We do not observe a shift of the cerianite diffraction peaks to higher Bragg angles; consequently the CuO is highly dispersed on the surface of the CeO_2 crystallites [9]. Recent studies reveal that transition-metal-doped ceria has enhanced oxygen and hydrogen storage capacities [26] due to the formation of anionic-defected solid solutions, which can be described by the formula $M_x^{2+}Ce_{1-x}^{4+}O_{2-y}^{2-}\square_y$, where $y < x$ at room temperature and $\square$ is an oxygen vacancy. However, cuprous oxide Cu_2O, having a primitive cubic lattice and a Cu^+ ionic radius equal to 0.115 nm, and CeO_2, having a fluorite structure with Ce^{4+} ionic radius equal to 0.111 nm, can form, at least in theory, a substitution solid solution [27,28]. During the reduction of this solid solution the reduced copper species (Cu^{1+} and Cu^0) are reoxidized by reduction of the Ce^{4+} ions in their vicinity to Ce^{3+} and the following redox equilibrium is established [9,18,29]:

$$Ce^{4+} + Cu^{1+} \leftrightarrow Ce^{3+} + Cu^{2+}.$$

This equilibrium has a buffer-like effect stabilising the presence of cationic copper species in the structure even in highly reductive atmosphere. The above scheme of copper oxide–ceria interactions indicates clearly that CuO/CeO_2 catalyst is bifunctionally promoted (both copper and ceria cooperate in the redox mechanism). Comparative spectroscopic studies between $CuO/CeO_2/Al_2O_3$, CuO/CeO_2, and CuO/Al_2O_3 have revealed that only a small and limited amount of copper interacting with ceria produces a large activity enhancement [30] toward CO oxidation, making the formation of a solid solution throughout the bulk of the CeO_2 phase highly improbable.

There are many examples of the CuO and CeO_2 synergistic effects. For example, pure CeO_2 catalyst exhibits two H_2 reduction peaks, one at 500 and one at 800 °C [31]. Pure CuO and Cu_2O catalysts have H_2 reduction peaks at approximately 180 and 300 °C [32]. It was found that when copper oxide and cerium oxide is prepared as a mixed $Cu_xCe_{1-x}O_{2-y}$ nanostructured catalyst, much better results are obtained. The latter oxide exhibits H_2 and CO reduction peaks well below 180 °C [17,33,34]. From the TPR experiments, it is clear that regarding the pure CeO_2 catalysts, temperatures higher than 700 °C are needed to mobilize and eliminate bulk lattice oxide ions. In contrast, in the present study it was shown that reduction several monolayers deep occurs already at 400 °C in case of the $Cu_{0.1}Ce_{0.9}O_{2-y}$ nanostructured catalyst. It is obvious then, that ceria is not present as a pure phase but has an amount of copper oxide dissolved in it which, even though perhaps small, is enough

to change its oxide ion transport properties and enable bulk reduction at 400 °C.

This synergism can also be measured by voltammetric measurements. Cyclic voltammetry studies coupled with temperature programmed reduction of a CuO/CeO_2 showed that redox potentials of the Cu^{2+}/Cu^{+} and Cu^{+}/Cu^{0} couples in a CeO_2 matrix are lower than those in unsupported CuO. The potential values indicated that Cu^{2+}/Cu^{+} and Cu^{+}/Cu^{0} couples in a CuO/CeO_2 matrix require less energy to be reduced than in the case of pure CuO [29]. The synergistic effect is also well demonstrated by the considerable lowering of the light-off temperature in the CO oxidation reaction without the presence of hydrogen over the CuO/CeO_2 when compared to separate CuO and CeO_2 catalysts [33]. Synergy between copper oxide and ceria in $Cu_xCe_{1-x}O_{2-y}$ at nanosize is also supported by the fact that physical mixture of $CuO + CeO_2$ has a higher light-off temperature than the $Cu_xCe_{1-x}O_{2-y}$ nanostructured catalyst [27].

4.3. The stability of $Cu_{0.1}Ce_{0.9}O_{2-y}$ nanostructured catalyst

The activity of freshly calcined and in situ oxidized $Cu_{0.1}Ce_{0.9}O_{2-y}$ nanostructured catalysts towards CO oxidation in excess hydrogen was found to irreversibly decrease in the first few hours when put on stream. When this rapid initial deactivation ceased, the catalyst was found to be very stable over long periods and even under several consecutive transient redox cycles at temperatures up to 400 °C.

Three possible methods of catalyst deactivation are possible: poisoning, coking, and solid-state transformations [35]. Coking of the catalyst was rejected, because no C-containing species were found on the catalyst surface (TOC analysis) after 1 week of operation under the lineout conditions. The latter was confirmed also by the fact that the gray/brown color of the catalyst remained unchanged.

The presence of H_2O in the reactor feed has no influence on the long-term stability of the same type of catalyst when prepared by coprecipitation and calcined at temperatures below 650 °C. When high enough temperatures are used (340 °C), complete CO conversion is achieved [27,33]. At lower temperatures, the presence of H_2O and/or CO_2 in the reactor feed only lowers the CO conversion (the suppression effect), but no influence on the long-term stability or on the selectivity of the catalyst can be detected [3]. Apart from this, catalyst poisoning by any component present in the feed would decrease the catalyst conversion monotonically to zero in most cases. Because of this, the fast initial catalyst deactivation in the reducing atmosphere is ascribed to solid-state transformation. The initial deactivation could be ascribed to some kind of copper redistribution (EPR-silent) process upon the first reduction [36], such as during the lineout treatment. This process was found also to be BET- and XRD-silent (Table 2 and Fig. 2) in the present study, but it can be perceived by kinetic measurements (Fig. 1). This behavior of the fresh catalyst when put on stream was explained also by the changes in the surface through changes in interfacial metal oxide–support interactions [37].

4.4. Mechanism of selective CO oxidation in excess hydrogen over the $Cu_{0.1}Ce_{0.9}O_{2-y}$ nanostructured catalyst

Oxygen involved in the oxidation reactions over oxide catalysts is present in two forms:

- surface-adsorbed oxygen, and
- lattice oxygen, which is a part of the oxide structure.

Oxygen adsorbed on oxide surfaces can be present in different forms. The superoxide ion form (O_2^-) decomposes further into a peroxide (O_2^{2-}) and an ion radical form, O^-. Lattice oxygen is present in the lattice ion form (O^{2-}). There always exists a balance between these forms, which moves to the right at higher temperatures [20]

$$O_2 \leftrightarrow O_2^- \leftrightarrow O_2^{2-} \leftrightarrow O^- \leftrightarrow O_{\text{lattice}}^{2-}.$$

In most papers on the oxidation reactions over metal oxides, "higher temperatures," are considered to be higher than 300 °C. However, in the case of transition metal oxide–ceria catalysts, including CuO/CeO_2, there is plenty of evidence that the surface lattice oxygen is involved in the oxidation reactions at much lower temperatures.

Besides oxygen, also hydrogen interacts with the oxide catalysts. A very recent H_2 TPR study over CuO/CeO_2 catalyst [34] reports that H_2 consumption started at around 60 °C with the first peak at 100 °C. A second H_2 consumption peak was found at around 150 °C, which overlapped completely with the water formation peak. One can conclude, that considerable amount of hydrogen was present on the catalyst surface at around 100 °C. However, first traces of water were formed above 100 °C. This is not a surprise, because apart from capability to store oxygen, the $CeCu_xO_y$ catalyst was proven to have hydrogen storage capacity as well [18]. These results are in a complete concordance with our steady-state kinetic results presented in Fig. 4 concerning H_2 oxidation reaction over the $Cu_{0.1}Ce_{0.9}O_{2-y}$ nanostructured catalyst. The H_2 oxidation started above 90 °C whether the CO was present or not in the reactor feed. This temperature is high enough for H_2 oxidation to start (the light-off temperature for an H_2 oxidation reaction over the $Cu_{0.1}Ce_{0.9}O_{2-y}$ nanostructured catalyst). It was found that at temperatures higher than 80 °C dissociation of molecular H_2 takes place on the $CeCu_xO_y$ catalyst [18].

Now let us suppose that CO (and H_2) oxidation reactions proceed only with the help of surface-adsorbed oxygen of any type (O_2^-, O_2^{2-}, or O^-) which spills over the surface, while CO or H_2 are waiting adsorbed on the metal domain of the catalyst. The example of that is Pt-group metal catalysts, for instance Pt/Al_2O_3. If these metal domains are of several atoms in size, one can expect that CO would adsorb on the surface preferentially, thus blocking

the access to hydrogen [38]. However, this is not the case in selective oxidation of CO in excess hydrogen over the oxide $Cu_{0.1}Ce_{0.9}O_{2-y}$ nanostructured catalyst, as was shown above and in Section 3.2, because the presence of CO does not suppress the H_2 oxidation reaction; on the contrary, it even promotes it. If CO and H_2 interfered also the onset of CO oxidation reaction would be changed in the presence of H_2 [38]. As seen from Fig. 3b, this is not the case with our catalyst. In addition to that, the mechanism, which presumes the simultaneous adsorption of CO and H_2 onto the metal domains of noble metal supported catalyst like Pt/Al_2O_3 must presume also that once enough CO is desorbed from the surface, it frees the adsorption places for the O_2 as well as for the H_2 to be adsorbed and both reactions of CO and H_2 oxidation start simultaneously [38]. Indeed, as soon as enough CO is desorbed from the surface of Pt/Al_2O_3 catalyst leaving space to O_2 (and H_2) to be adsorbed at around 130 °C, both CO and H_2 oxidation reactions start. Because H_2 is in excess, the selectivity is 0.2 at 130 °C, 0.5 at 220 °C, and down again to 0.3 at a temperature of 400 °C, with λ being equal to 1. At higher λ values, no drastical changes in selectivity were observed [39]. A completely different picture is found in the case of selective CO oxidation in excess hydrogen over the oxide $Cu_{0.1}Ce_{0.9}O_{2-y}$ nanostructured catalyst (Fig. 3) and was explained in Section 3.2. All those facts lead us to the conclusion that CO and H_2 do not compete for adsorption places on bigger metal domains or clusters. Instead of that mechanism, a redox mechanism as described already in brief in Section 3.3 is proposed for CO and H_2 oxidation over $Cu_{0.1}Ce_{0.9}O_{2-y}$ nanostructured catalyst.

As is widely known from the automobile three-way catalyst research, CeO_2 has multiple promoting effects in catalysis, where some of them are [40]:

- It promotes CO oxidation through employing lattice oxygen,
- It favors catalytic activity at the interfacial metal–support sites, and
- It stores and releases oxygen under oxygen lean and reach conditions.

In concordance with that, in situ redox studies showed that the abstraction of surface lattice oxygen and subsequently the formation of oxygen vacancies is the key step of CO oxidation reaction over different Cu/CeO_2 catalysts [16,17]. In the latter study, this mechanism was found to be present even at room temperature.

In general redox mechanism, when oxygenated product is desorbed from the surface (for instance, CO_2 or H_2O), oxygen vacancies are created. Those vacancies are then filled with oxygen from the gas phase, simultaneously reoxidizing the reduced cations. The incorporation of oxygen from the gas phase into the oxide surface does not necessarily take place at the same site where the reaction took place. On the contrary, the oxygen that refills the newly formed oxygen vacancy can be transported also through the catalyst lattice [13, p. 134]. Indeed, substantial amounts of bulk lattice oxygen can be extracted from the $Cu_{0.1}Ce_{0.9}O_{2-y}$ nanostructured catalyst by CO reduction at 400 °C (Fig. 8). Tschöpe et al. report for similar $Cu_{0.15}Ce_{0.85}O_{2-y}$ catalysts the quantity of oxygen extracted from the surface by CO reduction, measured gravimetrically at 200 °C, to be about 1.85% weight [41]. This amount of oxygen would be enough to reduce all Cu^{2+} into Cu^0 and to reduce the surface of ceria. Poulston et al. have shown by spectroscopic study that the diffusion of lattice oxygen in CuO and Cu_2O catalysts at temperatures around 130 °C could readily be observed during H_2 reduction [42].

If the catalyst is to be reduced in the bulk phase, it must also exhibit high ionic and electronic conductivity in order to cope with charge transfers. It was found that ceria-based oxides with fluorite-type structure (as is also the case in the $Cu_{0.1}Ce_{0.9}O_{2-y}$ nanostructured catalyst) have remarkably high electrical and ionic conductivity. This high electrical and ionic conductivity gave them the name "solid electrolytes" [43]. This is the basis for the so-called ionosorption model of oxygen. It can be summarized as follows [44]:

- Chemisorption of oxygen is low on defect-free surfaces of insulating materials.
- The amount of chemisorbed oxygen increases with donor doping or surface defect concentration, both generating free electronic charge carriers.
- The degree of ionization of oxygen increases with defect concentration or electron density.

In other words, doubly ionized oxygen vacancies are created upon lattice oxygen extraction and two electrons become mobile, giving rise to electrical conductivity. This was experimentally confirmed [45]: electronic conductivity of the CeO_{2-x} catalyst increased several orders of magnitude when the atmosphere was changed from oxidative to reductive. Besides from that, it was shown that for the $Ce_{0.69}Gd_{0.31}O_{2-y}$ catalyst [46], the activation energy for oxygen ion diffusivity measured by isotope tracer studies on a single crystal had similar value as the one obtained from measurements of electrical conductivity when converted to oxygen self diffusion coefficient using the Nernst–Einstein equation. This suggests that the two processes are in fact very similar in nature. As expected, the lattice oxygen diffusion coefficient is independent of oxygen partial pressure for the $Ce_{0.9}Gd_{0.1}O_{2-y}$ catalyst [47].

In contrast to the oxygen diffusion coefficient, the oxygen surface exchange coefficient (the coefficient of oxygen exchange between gas phase and catalyst surface) was found to vary as $P_{O_2}^{0.25}$ between 10 and 1000 mbar oxygen partial pressure in hydrogen over the same catalyst, measured at a temperature of 800 °C [47]. The exponent 0.25 over oxygen partial pressure is in fact very similar to the exponent $n = 0.2 \pm 0.05$ (Table 3 and Fig. 5b) which was obtained

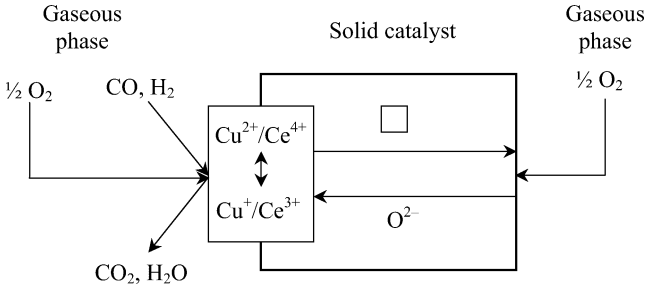

Fig. 9. Scheme of the Mars and van Krevelen mechanism for selective CO oxidation in excess hydrogen over the $Cu_{0.1}Ce_{0.9}O_{2-y}$ nanostructured catalyst. The enhanced reactivity at the interface of CuO and CeO_2 is presented. The reoxidation of the catalyst can proceed by two parallel paths: directly from the gaseous phase or by the diffusion of oxygen through the bulk of the catalyst crystal lattice. The latter path is more pronounced at higher temperatures.

for the Mars and van Krevelen kinetic model (Eq. (5)) at temperatures below 100 °C and can be interpreted as an exponent for the reoxidation of the surface.

As a general rule, higher reactivities of CO compared to H_2 will be achieved over metal oxide catalysts, when [13, p. 306]:

- higher oxygen–surface bonding energies are present,
- lower reaction temperatures are used, and
- higher ratios of O_2/(CO or H_2) are used.

In the light of all said in the above discussion, we propose the following tentative scheme (Fig. 9) for the selective CO oxidation over the $Cu_{0.1}Ce_{0.9}O_{2-y}$ nanostructured catalyst: CO and H_2 adsorb on the copper/ceria interfacial region of the catalyst, the most reactive places for both CO and H_2 oxidation reactions. In the present paper it is proposed that CO (and H_2) use mostly copper cations as the adsorption sites [20], while cerium oxide must also be present in the close vicinity [18]. As explained earlier in the text, it is proposed that copper oxide might also form a solid solution with cerium oxide at least in the form of small intergrowths at the interface, which are XRD-invisible. In this concerted mechanism of copper and cerium oxide, the copper cation has the following role: it is the adsorption site for the CO (and H_2). When either of the two reactants is adsorbed on the copper cation, it extracts oxygen from the surface and copper is reduced from Cu^{2+} to Cu^{+}. The cerium cation, which lies next to the copper cation, can supply additional oxygen atoms from the catalyst lattice while it reduces itself simultaneously from the Ce^{4+} to the Ce^{3+} form. Cerium oxide acts as an oxygen supplier when it is needed at the place of reaction. Only a single copper ion is enough to convert one molecule of CO (or H_2) into CO_2 (or H_2O), respectively. When the product molecule is desorbed, the site becomes available for next reactant molecule, either CO or H_2. Upon extraction of surface oxygen from the catalyst lattice, oxygen vacancies may be refilled directly from the gas phase or by oxygen diffusion through the bulk of the catalyst. The latter mechanism is observed at higher temperatures.

The behavior of the $Cu_{0.1}Ce_{0.9}O_{2-y}$ nanostructured catalyst in the CO or H_2 oxidation reaction can be explained by the redox mechanism. For instance, at a temperature of 105 °C, the selectivity of the catalyst is roughly around 95% in all cases where the excess of hydrogen is present in the reactor feed (Fig. 3). The reason for this is that the onsets of CO and H_2 oxidation reactions are more than 50 °C apart. The H_2 oxidation reaction is simply too slow at that temperature due to the lack of reactive hydrogen species. At the temperature of 155 °C, the selectivity obtained over the $Cu_{0.1}Ce_{0.9}O_{2-y}$ nanostructured catalyst (71.5%, Fig. 3a) is still higher than that obtained over the Pt/Al_2O_3 catalysts at 220 °C (around 50% [39]). In spite of the great difference in partial pressures of the reactants, being 0.01 bar for CO and 0.985 bar for H_2, respectively, carbon monoxide is more able to extract oxygen from the $Cu_{0.1}Ce_{0.9}O_{2-y}$ nanostructured catalyst lattice than hydrogen. As already observed in [24], CO is a better reducing agent than H_2 (at least for the CeO_2 catalyst).

The enhancement of water production that we have observed over the $Cu_{0.1}Ce_{0.9}O_{2-y}$ nanostructured catalyst when the CO was added into the feed gas containing H_2 and O_2 can be explained as follows: since the surface is more reduced when the CO is present in the reactor feed gas, more oxygen vacancies are formed, and as a consequence the concentration of reactive hydrogen species increases and the catalyst is more reactive for the hydrogen oxidation reaction.

Liu and Flytzani-Stephanopoulos as well as Mars and van Krevelen kinetic models can almost equally well predict the rate of steady-state CO oxidation in excess of hydrogen over the $Cu_{0.1}Ce_{0.9}O_{2-y}$ nanostructured catalyst at temperatures between 48 and 90 °C as presented in Fig. 7. The steady-state kinetic model proposed by Liu and Flytzani-Stephanopoulos [20] assumes that no lattice oxygen is involved in the CO oxidation reaction over the $Cu_{0.1}Ce_{0.9}O_{2-y}$ nanostructured catalyst. In the first place, this is in contrast with the findings of the in situ spectroscopic studies [16,17], where lattice oxygen was proved to be involved in the reaction. The Mars and van Krevelen mechanism, in contrast, was derived on the basis of the redox mechanism [19]. When these two models are compared, taking into account their theoretical basis, the authors of the present study stay in favor of the Mars and van Krevelen kinetic model.

Neither of those two models takes into account the possibility of bulk lattice oxygen being involved in the reaction. At present it cannot be explained how much of bulk lattice oxygen is involved in the CO oxidation reaction over $Cu_{0.1}Ce_{0.9}O_{2-y}$ nanostructured catalysts at reaction temperatures as low as 50 °C. This will be the subject of further transient as well as tracer studies. If there is bulk lattice oxygen present in the CO oxidation reaction at 50 °C, the constant for the reoxidation of the surface, k_{O_2}, in the Mars and van Krevelen model is in fact a lumped constant,

which does not differentiate between the reoxidation of the catalyst surface layer directly by the gas phase oxygen and its reoxidation through the bulk of the catalyst. These questions remain open for further studies.

5. Conclusions

In the present study we have shown that:

- The $Cu_{0.1}Ce_{0.9}O_{2-y}$ nanostructured catalyst prepared by the sol–gel method is a very efficient selective CO oxidation catalyst even under highly reducing conditions, which are present in a PROX reactor.
- The $Cu_{0.1}Ce_{0.9}O_{2-y}$ nanostructured catalyst is energy-efficient toward the PEM fuel cell technology, because it oxidizes CO with 100% selectivity close to the PEM fuel cell working temperature (the influence of CO_2 and H_2O in the reactor feed was not studied here).
- The selective CO oxidation follows the redox mechanism described by the Mars and van Krevelen model over wide range of partial pressures of CO and O_2. Although the modified Langmuir–Hinshelwood model introduced by Liu et al. almost equally well describes the steady-state kinetics, the authors of the present paper favor the former model because of the difference in physical nature and fundamental assumptions between these two models.
- The very high selectivity of the $Cu_{0.1}Ce_{0.9}O_{2-y}$ nanostructured catalyst is ascribed to the better ability of CO to extract oxygen from the catalyst surface compared to H_2.
- After initial deactivation, the $Cu_{0.1}Ce_{0.9}O_{2-y}$ nanostructured catalyst exhibits stable operation under medium and severe reducing conditions.
- The reduction of the $Cu_{0.1}Ce_{0.9}O_{2-y}$ nanostructured catalyst by CO at 400 °C is estimated to occur several monolayers deep in the ceria phase. This is possible only if a certain amount of copper oxide is dissolved in ceria at the interface. The involvement of bulk lattice oxygen in the CO (and H_2) oxidation at lower temperatures is a subject of further studies.
- Those performances are obtained with a catalyst that contains cheap copper and cerium oxides rather than costly noble metals.
- The catalyst precursor prepared in the form of a stable sol is convenient for deposition on any geometry of catalyst support or on the reactor walls.

Acknowledgments

The authors gratefully acknowledge the financial support of the Ministry of Education, Science and Sport of the Republic of Slovenia through Grant P0-0521-0104. They also thank one of the referees for detailed remarks, which helped to improve the manuscript.

References

[1] M.J. Kahlich, H.A. Gasteiger, R.J. Behm, J. Catal. 171 (1997) 93.
[2] M.J. Kahlich, H.A. Gasteiger, R.J. Behm, J. Catal. 182 (1999) 430.
[3] G. Avgouropoulos, Ch. Ioannides Papadopoulou, J. Batista, S. Hočevar, H.K. Matralis, Catal. Today 75 (2002) 157.
[4] C.D. Dudfield, R. Chen, P.L. Adcock, J. Power Sources 85 (2000) 237.
[5] S. Hočevar, J. Batista, H. Matralis, T. Ioannides, G. Avgouropoulos, PCT Application No. PCT/SI01/00005, 2001.
[6] G. Avgouropoulos, T. Ioannides, H.K. Matralis, J. Batista, S. Hočevar, Catal. Lett. 73 (2001) 33.
[7] K. Sekizawa, S. Yano, K. Eguchi, H. Arai, Appl. Catal. A Gen. 169 (1998) 291.
[8] Y. Liu, T. Hayakawa, K. Suzuki, S. Hamakawa, Catal. Commun. 2 (2001) 195.
[9] S. Hočevar, J. Batista, J. Levec, J. Catal. 184 (1999) 39.
[10] S. Hočevar, U. Opara Krašovec, B. Orel, A.S. Arico, H. Kim, Appl. Catal. B Env. 28 (2000) 113.
[11] M. Flytzani-Stephanopoulos, MRS Bull. November (2001) 885.
[12] F.M. Dautzenberg, ACS Sympos. Ser. 411 (1989) 99.
[13] A. Bielanski, J. Haber, Oxygen in Catalysis, Dekker, New York, 1991.
[14] G.I. Golodets, Heterogeneous Catalytic Reactions Involving Molecular Oxygen, in: Studies in Surface Science and Catalysis, Vol. 15, Elsevier, Amsterdam, 1983.
[15] A. Tschöpe, W. Liu, M. Flytzany-Stephanopoulos, J.J. Ying, J. Catal. 157 (1995) 42.
[16] P.G. Harrison, I.K. Ball, W. Azelee, W. Daniell, D. Goldfarb, Chem. Mater. 12 (12) (2000) 3715.
[17] A. Martinez-Arias, M. Fernandez-Garcia, O. Galvez, J.M. Coronado, J.A. Anderson, J.C. Conesa, J. Soria, G. Munuera, J. Catal. 195 (2000) 207.
[18] C. Lamonier, A. Ponchel, A. D'Huysser, L. Jalowiecki-Duhamel, Catal. Today 50 (1999) 247.
[19] P. Mars, D.W. van Krevelen, Chem. Eng. Sci. 3 (1954) 41 (Spec. Suppl.).
[20] W. Liu, M. Flytzani-Stephanopoulos, J. Catal. 153 (1995) 317.
[21] D.A. Skoog, D.N.J. West, F.J. Holler, in: Fundamentals of Analytical Chemistry, 6th ed., Saunders, Fort Worth, TX, 1992, p. 34.
[22] V. Ponec, Z. Knor, S. Černy, in: Adsorption on Solids, Buttherwords, London, 1974, p. 541.
[23] A. Laachir, V. Perrichon, A. Badri, J. Lamotte, et al., J. Chem. Soc. Faraday Trans. 87 (1991) 1601.
[24] A. Badri, J. Lamotte, J.C. Lavalley, A. Laachir, V. Perrichon, O. Touret, G.N. Sauvion, E. Quemere, Eur. J. Solid State Inorg. Chem. 28 (1991) 445.
[25] Y. Li, Q. Fu, M. Flytzani-Stephanopoulos, Appl. Catal. B Env. 27 (2000) 179.
[26] G. Wrobel, C. Lamonier, A. Bennani, A. D'Huysser, A. Aboukaïs, J. Chem. Soc. Faraday Trans. 92 (1996) 2001.
[27] W. Liu, M. Flytzani-Stephanopoulos, J. Catal. 153 (1995) 304.
[28] M. Fernández-Garcia, E. Gómez Rebollo, A. Guerrero Ruiz, J.C. Conesa, J. Soria, J. Catal. 172 (1997) 146.
[29] P. Bera, S. Mitra, S. Sampath, M.S. Hegde, Chem. Commun. (2001) 927.
[30] A. Martinez-Arias, J. Soria, R. Cataluña, J.C. Conesa, C.V. Cortés, Stud. Surf. Sci. Cat. 116 (1998) 591.
[31] H.C. Yao, Y.F. Yu Yao, J. Catal. 86 (1984) 254.
[32] G. Fierro, M. Lo Jacono, M. Inversi, P. Porta, R. Lavecchia, F. Cioci, J. Catal. 148 (1994) 709.
[33] W. Liu, M. Flytzani-Stephanopoulos, Chem. Eng. J. 64 (1996) 283.
[34] P. Zimmer, A. Tschöpe, R. Birringer, J. Catal. 205 (2002) 339.

[35] G.F. Froment, K.B. Bischoff, in: Chemical Reactor Analysis and Design, Wiley, New York, 1990, p. 219.
[36] A. Martinez-Arias, M. Fernandez-Garcia, J. Soria, J.C. Conesa, J. Catal. 182 (1999) 367.
[37] J.B. Wang, D.-H. Tsai, T.-J. Huang, J. Catal. 208 (2002) 370.
[38] S.H. Oh, R.M. Sinkevitch, J. Catal. 142 (1993) 254.
[39] D.H. Kim, M.S. Lim, Appl. Catal. A Gen. 224 (2002) 27.
[40] J. Kašpar, P. Fornasiero, M. Graziani, Catal. Today 50 (1999) 285.
[41] A. Tschöpe, M.L. Trudeau, J.Y. Ying, J. Phys. Chem. B 103 (1999) 8858.
[42] S. Poulston, P.M. Parlett, P. Stone, M. Bowker, Surf. Interface Anal. 24 (1996) 811.
[43] H. Inaba, H. Tagawa, Solid State Ionics 83 (1996) 1.
[44] A. Tschöpe, D. Schaadt, R. Birringer, J.Y. Ying, NanoStruct. Mater. 9 (1997) 423.
[45] A. Tschöpe, J.Y. Ying, H.L. Tuller, Sensors Actuat. B 31 (1996) 111.
[46] E. Ruiz-Trejo, J.D. Sirman, Y.M. Baikov, J.A. Kilner, Solid State Ionics 113–115 (1998) 565.
[47] J.A. Lane, J.A. Kilner, Solid State Ionics 136–137 (2000) 927.